

EVAPORATION OVER A HETEROGENEOUS LAND SURFACE

The EVA-GRIPS Project

BY H.-T. MENGELKAMP, F. BEYRICH, G. HEINEMANN, F. AMENT, J. BANGE, F. BERGER, J. BÖSENBERG, T. FOKEN, B. HENNEMUTH, C. HERET, S. HUNEKE, K.-P. JOHNSEN, M. KERSCHGENS, W. KOHSIEK, J.-P. LEPS, C. LIEBETHAL, H. LOHSE, M. MAUDER, W. MEIJNINGER, S. RAASCH, C. SIMMER, T. SPIEB, A. TITTEBRAND, J. UHLENBROCK, AND P. ZITTEL

A field experiment combined with numerical studies provides a better understanding of the area-averaged evaporation and leads to improved parameterization schemes.

The earth's surface is characterized by spatial heterogeneity over a wide range of scales, as can be seen by examining soil and topographic maps. This heterogeneity affects the exchange of momentum, heat, and water between the land surface and atmosphere. Specification of these processes is vital for climate and weather forecast models. However, the horizontal resolution of present-day numerical atmospheric models is too coarse to explicitly capture the effects of surface heterogeneity, which therefore

are commonly parameterized as an integral part of the host model's land surface scheme. The problem of subgrid-scale variability is particularly relevant in modeling evapotranspiration because soil moisture may vary on scales as small as a few meters. In combination with the natural heterogeneity of vegetation, orography, and nonuniform precipitation on larger scales, this may result in a relationship between regional evapotranspiration and area-averaged soil moisture that is fundamentally different from the

AFFILIATIONS: MENGELKAMP, HUNEKE, JOHNSEN, LOHSE—GKSS Research Center, Geesthacht, Germany; BEYRICH, LEPS—Meteorological Observatory—Lindenberg, German Meteorological Service (DWD), Tauche, Germany; AMENT, SIMMER—Meteorological Institute, University of Bonn, Bonn, Germany; HEINEMANN, KERSCHGENS—Institute for Geophysics and Meteorology, University of Cologne, Cologne, Germany; BANGE, SPIEB, ZITTEL—Institute for Aerospace Systems, Technical University Braunschweig, Braunschweig, Germany; FOKEN, LIEBETHAL, MAUDER—Department of Micrometeorology, University Bayreuth, Bayreuth, Germany; HENNEMUTH, BÖSENBERG—Max-Planck-Institute for Meteorology, Hamburg, Germany; BERGER, HERET, TITTEBRAND—Institute of Hydrology and Meteorology, Dresden University of Technology,

Tharandt, Germany; RAASCH, UHLENBROCK—Institute for Meteorology and Climatology, University Hannover, Hannover, Germany; KOHSIEK—KNMI, De Bilt, Netherlands; MEIJNINGER—Wageningen University, Wageningen, Netherlands
CORRESPONDING AUTHOR: Heinz-Theo Mengelkamp, GKSS Research Center, Institute for Coastal Research, D-21502 Geesthacht, Germany
E-mail: mengelkamp@gkss.de

The abstract for this article can be found in this issue, following the table of contents.

DOI:10.1175/BAMS-87-6-775

In final form 24 January 2006
©2006 American Meteorological Society

relationship at a particular point (Wetzel and Chang 1988). Avissar and Pielke (1989) and Pielke and Avissar (1990) have summarized observations that demonstrate the significant impact of land surface heterogeneity on the atmosphere.

Numerous studies describe different ways of considering subgrid-scale land surface heterogeneities in atmospheric models (e.g., Arain et al. 1996; Avissar 1992; Chebouni et al. 1995; Koster and Suarez 1992a,b; Lhomme et al. 1994; Li and Avissar 1994; Noilhan et al. 1997; Sellers et al. 1997a; Shuttleworth et al. 1997).

Basically, three methods have been developed. The “tile” approach (e.g., Li and Avissar 1994; Fig. 1) describes the heterogeneity inside a model grid cell in terms of a finite number of homogeneous tiles or “patches,” representing the major vegetation and soil types. The grid cell fluxes are the averages of the tile fluxes weighted by their fractional area. For the “mosaic” approach (e.g., Koster and Suarez 1992a; Fig. 1), the low-resolution model grid cell is subdivided into a regular, smaller high-resolution grid. While the coarse grid for the host model is preserved, the soil–vegetation–atmosphere transfer (SVAT) scheme is run for the smaller grid. The averages of the subgrid fluxes represent the fluxes on the coarse grid. In a SVAT scheme, a number of parameters are used to describe the soil and vegetation characteristics inside the grid cell. These parameters are usually selected in correspondence to the most common vegetation and soil types within the grid cell. For the “effective parameter” approach (e.g., Arain et al. 1996), the single vertical description of the exchange processes is retained and the parameters are selected to provide a realistic description of the grid cell–averaged surface fluxes. Because of the highly nonlinear interaction between the soil, the vegetation, and the atmosphere, there is no general rule for the derivation of suitable parameters and averaging procedures.

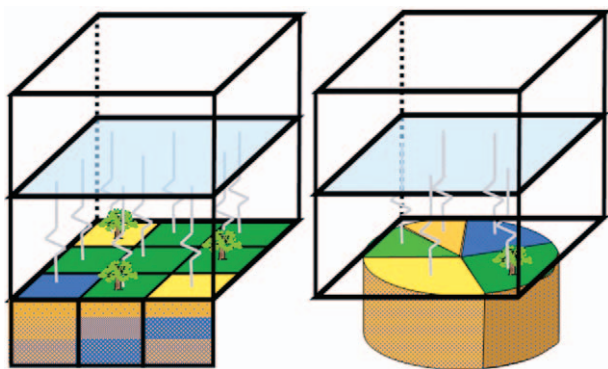


FIG. 1. Sketch of (left) mosaic and (right) tile approaches.

The Evaporation at Grid and Pixel Scale (EVA-GRIPS) project was aimed at investigating parameterization schemes for area-averaged evaporation over a heterogeneous land surface at the scale of a grid box of a regional numerical weather prediction or climate model. Model studies were combined with a comprehensive field campaign over an area typical for northern Central Europe and the southern drainage basin of the Baltic Sea. EVA-GRIPS was funded under the auspices of the German Climate Research Program for the period from 2002 to 2004 as a contribution to the Baltic Sea Experiment (BALTEX; Raschke et al. 2001; Mengelkamp 2004). BALTEX represents 1 of the 11 continental-scale experiments in the frame of the Global Energy and Water Cycle Experiment (GEWEX; information available online at www.gewex.org).

Over the past decade, a number of field campaigns have been conducted similar to the experimental component of EVA-GRIPS (Table 1). When compared to these programs, EVA-GRIPS differs in scale (meso- γ versus meso- β), area coverage (grid cell versus watershed), heterogeneity, and climate conditions. Moreover, within EVA-GRIPS, a strong emphasis is put on numerical modeling directly linked to the field measurements. The experimental dataset is used to verify parameterization schemes in land surface models.

The activities of the EVA-GRIPS project focused on an area of about 20 km \times 20 km around the Meteorological Observatory Lindenberg (MOL) of the German Meteorological Service [*Deutscher Wetterdienst* (DWD)] in northeastern Germany in a rural environment about 65 km southeast of Berlin. The landscape in this area has been formed by the inland glaciers during the last ice age, exhibiting a slightly undulating surface with height differences of about 80–100 m over distances of about 10–15 km, with a number of small- and medium-sized lakes embedded. The land use is dominated by forest and agricultural fields (40%–45% each); lake coverage is 6%–7%, and villages and traffic roads cover less than 4%. The forest is mainly situated in the western part of the area, while agriculture is dominant in the eastern part (Fig. 2). This mixture of surface types is rather typical for the whole region and even for larger parts of northern Central Europe.

THE LITFASS-2003 EXPERIMENT. The project activities in EVA-GRIPS could benefit from experiences gained during the Lindenberg Inhomogeneous Terrain—Fluxes between Atmosphere and Surface: A Long-term Study (LITFASS) project of the DWD (Beyrich et al. 2002a). This project was designed in the

TABLE 1. Some major field campaigns with focus on vegetation–atmosphere exchange and boundary layer processes.

	Reference	Special focus	Location	Lat	Climate	Vegetation	Scale
Hydrological Atmospheric Pilot Experiment (HAPEX)-Modelisation du Bilan Hydrique (MOBILHY)	André et al. (1988)	Hydrological balance	France	44°N	Temperate, marine influence	Heterogeneous (forest/agriculture)	Meso-β
HAPEX in the Sahel (HAPEX-SAHEL)	Goutorbe et al. (1994)	Hydrological balance	Niger	13°–14°N	Semiarid	Grass steppe, savanna	Meso-β
First International Satellite Land Surface Climatology Project (ISLSCP) Field Experiment (FIFE)	Sellers and Hall (1992)	Satellite ground segment	Kansas	39°N	Temperate	Mainly grassland	Meso-γ
Echival Field Experiment in a Desertification Threatened Area (EFEDA)	Bolle et al. (1993)	Desertification	Spain	39°N	Mediterranean, continental character	Agriculture	Meso-β
Boreal Ecosystem-Atmosphere Study (BOREAS)	Sellers et al. (1997b)	Cold climate	Canada	54°–56°N	Boreal	Boreal forest	Meso-β/α
Northern Hemisphere Climate Processes Land Surface Experiment (NOPEX)	Halldin et al. (1998)	Hydrology	Sweden	60°N	Transition from temperate to boreal	Heterogeneous (boreal forest, farmland, mires, lakes)	Meso-β
NOPEX Winter Experiment (NOPEX WINTEX)	Halldin et al. (2001)	Cold climate winter conditions	Finland	67°N	Boreal	Boreal forest/tundra	Meso-γ
Cooperative Atmosphere-Surface Exchange Study (CASES)-99	LeMone et al. (2000)	Stable boundary layer, CASES-99	Kansas	37°N	Temperate	Mainly grassland	Meso-γ/β
EVA-GRIPS/LITFASS 2003	Beyrich et al. (2006)	Area averaging of evaporation	Germany	52°N	Temperate, transition from marine to continental influence	Heterogeneous (forest, farmland, lakes)	Meso-γ

1990s in order to develop and test a strategy for the determination and parameterization of the area-averaged turbulent fluxes of heat, momentum, and water vapor over a heterogeneous landscape at the meso-γ scale, using a suitable combination of measurements and high-resolution nonhydrostatic modeling.

The major field survey in EVA-GRIPS took place during the main growing season between 19 May and 17 June 2003. An aerial view across the heterogeneous landscape and the placement of the ground-based instrumentation is shown in Fig. 3. The instrumentation comprised of the following:

- 13 micrometeorological sites over eight land use types (meadow, maize, rye, triticale, barley, rape, pine forest, open water) with eddy correlation sensors for the turbulent fluxes; standard equipment for wind speed, temperature, humidity, and radiation fluxes; and sensors to measure vertical profiles of soil parameters;
- three large-aperture optical scintillometers (LAS; Beyrich et al. 2002b) and a microwave scintillometer (MWS), set up along three different paths over distances of 3–10 km;
- the combination of a differential absorption lidar (DIAL) and a wind lidar for the performance of

- synchronized high-resolution (10-s sampling rate) measurements of water vapor and vertical velocity profiles (Bösenberg 1998);
 - the turbulence probe Helipod (Bange and Roth 1999; Bange et al. 2002), a sonde carried by a helicopter to perform measurements of temperature, humidity, and wind at a 100-Hz sampling rate, which was operated during 23 flights covering more than 60 h of measurements; and
 - an infrared camera for surface temperature mapping operated on board a Tornado aircraft of the German Air Force
- Satellite images [*Landsat-7* Enhanced Thematic Mapper (ETM) and the National Oceanic and Atmospheric Administration (NOAA) Advanced Very High Resolution Radiometer (AVHRR)] completed the set of observations. The spatial scales of



Fig. 2. Location of the experimental area roughly 65 km southeast of Berlin. (right) The Landsat picture (copyright GEOSPACE Herold, 1997 Herold Business Data AG/GEOSPACE Beckel Satellitenbilddaten GmbH) gives an impression of the landscape heterogeneity inside nine grid cells of the weather forecast model of DWD (LM). Each grid cell covers an area of 7 km × 7 km. The western part is dominated by forested areas and the eastern part by farmland.

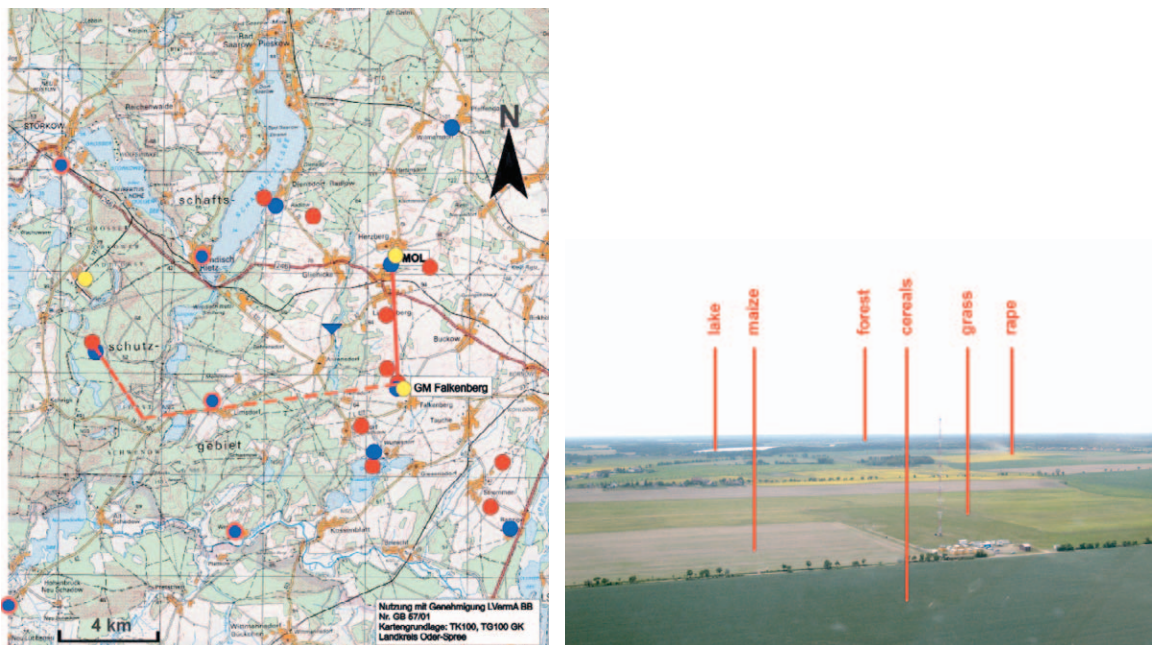


Fig. 3. (left) LITFASS 2003 area with the measurement stations and (right) an aerial view of the central site and its surrounding. Surface-based measurements of the turbulent fluxes were taken at 13 sites (red dots), ground-based remote sensing systems were operated at 3 sites (yellow dots), the blue symbols mark the position of rain gauges of a regional precipitation network (surrounded by a red ring where global radiation is measured in addition), and the red lines indicate the long-distance scintillometer paths.

this suite of measurement systems (Fig. 4) covered five orders of magnitude ($10^{-1} \dots 10^4$ m) for the sampling scale and three orders of magnitude ($10^1 \dots 10^4$ m) for the footprint scale, respectively.

Combined flights of the Tornado aircraft and the Helipod took place on 6 days. The grayscale pictures taken with the infrared camera on board the Tornado aircraft were calibrated with surface temperatures measured with the Helipod on a grid-like flight pattern and with those measured directly at the micrometeorological stations. High-resolution (1 m) surface temperature maps indicate a large heterogeneity regarding the surface temperature, even across fields that appeared to be homogeneous in the visible (Fig. 5). This is basically due to the large variation in soil moisture, even at homogeneously vegetated surfaces, and it may explain differences in



FIG. 4. Instrumentation during the LITFASS 2003 experiment (top left, left to right) Tornado aircraft, lidar and wind profiler Radio Acoustic Sounding System (RASS) at the central site (GM), helicopter with Helipod; (second row, left to right) GM with 99-m tower, and laser scintillometer over a maize field; (third row, left to right) micrometeorological station at a lake, soil sensors, forest tower; (bottom row, left to right) micrometeorological station over barley, large-aperture scintillometer path, boundary layer wind profiler at MOL.



FIG. 5. (center) Infrared image of the area around the central site taken from a Tornado RECCE aircraft of the German Air Force and surface temperatures from the (left) Helipod, which were used to calibrate the infrared images and the calibrated infrared surface temperature from (right) the combination of Tornado and Helipod measurements. The reverse “L”-shaped central experimental site GM of roughly 300 m × 200 m size can be identified in the center picture and in the lower left quadrant of the right-hand picture. Temperatures in the left-hand picture range from 20° (blue) to 55°C (red).

the fluxes over similar vegetation and soil types, and even at different locations on the same field.

Special attention was given to quality assurance and quality control issues. This included, for example, intercomparisons of the turbulence, radiation, and soil sensors during a preexperiment. The humidity profiling systems (radiosonde, DIAL, microwave radiometer profiler) were regularly controlled against each other. A laboratory calibration procedure was set up for the fast-response hygrometers, and all hygrometers from the different groups were calibrated according to this unified procedure prior to and after the experiment. Calculation of the turbulent fluxes was realized with identical software applied to all eddy covariance measurements (Foken et al. 2004). This ensured comparability of the computed fluxes with respect to data treatment and correction algorithms and a defined high quality of the derived turbulent fluxes. The major components of this flux computation and quality control system comprise the detection and removal of spikes in the raw data time series; corrections for transducer-induced flow distortion and crosswind effects on the sonic anemometer measurements; a planar-fit coordinate transformation (Wilczak et al. 2001); and corrections for the effects of high-frequency spectral losses due to sensor geometries (line averaging, spatial separation), for oxygen cross sensitivity (in case of Krypton hygrometers), for buoyancy effects on the sonic temperature, and for volume–mass conversion and density effects on the trace gas (water vapor) fluxes. Finally, the computed fluxes were checked for stationarity and

the plausibility of integral turbulence characteristics, and a footprint analysis was performed for each of the micrometeorological sites.

Land surface schemes inherently assume closure of the surface energy balance. However, it is well known that measurements usually do not show a closure of the surface energy balance (e.g., Foken and Oncley 1995; Wilson et al. 2002). When comparing the sum of the sensible and latent heat flux with the difference of net radiation and soil heat flux from 30-min-measured averages, the rmse of all stations varies between 70 and 130 $W m^{-2}$, and the bias (mean absolute residual) varies between 57 and 107 $W m^{-2}$ (Johnsen et al. 2005). There is a year-long discussion about the source for the energy balance closure gap. Here, we will only mention that the flux measurements show a balance closure gap of typically 20%–25% of the available energy for 30-min averages (Fig. 6). The best closure was achieved for the short grass at the central site (GM) while the highest residual was found for the A4 (maize) and A9 (rape) sites.

Results of the experimental determination of the latent heat (water vapor) fluxes from measurements using different techniques are illustrated in Fig. 7 for 25 May 2003. A flux composite for the farmland part of the area was derived by suitably averaging the data from the eddy covariance measurements at the 10 micrometeorological stations, weighting them according to the relative frequency of occurrence of the different types of crops across the study region (Beyrich et al. 2006; manuscript submitted to *Boundary Layer Meteor.*). These composites could then be compared to the area-averaged fluxes directly determined from the scintillometer and Helipod measurements.

Ranges of uncertainty estimated for each of the different flux values are also indicated. Referring to the Helipod data, these represent the statistical error of the derived fluxes. In the case of the flux composite, they represent the variability of the local fluxes among the different eddy covariance sites or the uncertainty derived from the sensor comparison experiment (whichever is larger). In case of the scintillometer data they represent the methodological uncertainty (due to, e.g., the choice of similarity coefficients).

While the three different flux estimates appeared to be widely consistent in the case of the sensible

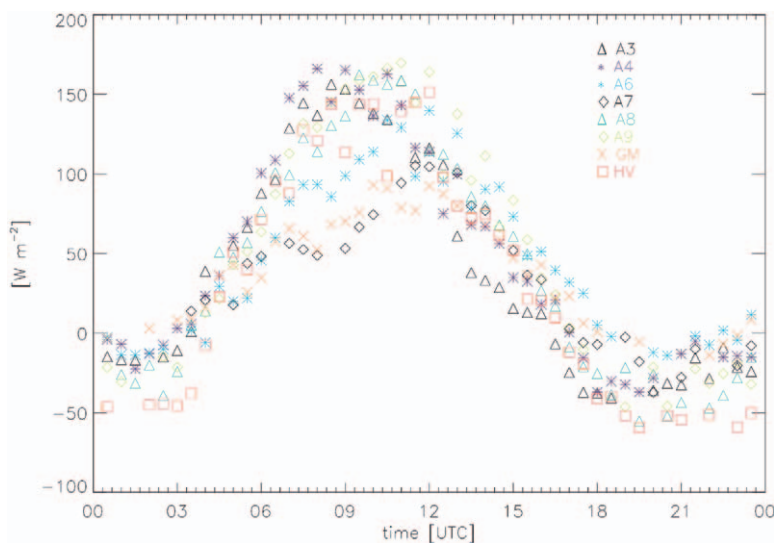


FIG. 6. Mean diurnal cycle of the energy balance closure gap at selected sites (A3: barley, A4: maize, A6: maize, A7: rape, A8: triticale, A9: rape, GM: grass, HV: pine forest) based on 30-min averages.

heat flux (not shown here), larger deviations were found between the different types of measurements for the latent heat flux. Systematically higher latent heat fluxes were derived from the scintillometer data when compared to the composite of the eddy covariance measurements, even if many of the scintillometer-based fluxes are still within the uncertainty range of the composite. Quite a deal of scatter has to be noticed for the Helipod fluxes. Interpretation of these differences has to be subject of further data analysis. The farmland composite fluxes fit well with downward-extrapolated vertical profiles of latent heat flux, which were determined by a combination of two lidar systems (Linné et al. 2005). Figure 7 reveals significant differences in the magnitude of the fluxes between the major land use classes (forest and low vegetation/farmland). A large variation was also found between the different types of agricultural farmland (cereals, rape, maize, and grassland; not shown here). During daytime, these differences exceed the estimated uncertainty of the measured fluxes (except for some of the Helipod measurements) and can therefore be considered significant.

A complete quality-controlled dataset of area-averaged surface fluxes from the 4-week period (with a data coverage of more than 80%) is now available for the forcing and validation of numerical models and flux-averaging strategies, and also for investigating algorithms to derive surface energy fluxes from satellite data.

NUMERICAL STUDIES. Three different uncoupled SVAT schemes were applied to examine the consistency of simulated and measured turbulent fluxes over various vegetation types and the adequacy of commonly used vegetation and soil parameters. Area-averaged fluxes were determined from a composite of the surface measurements and were compared to those fluxes simulated by three weather forecast and mesoscale models for the respective grid cells. The influence of mesoscale structures on the turbulent fluxes in the planetary boundary layer was studied by use of a large-eddy simulation model.

SVAT MODELING. Commonly, soil and vegetation characteristics are defined in SVAT models by

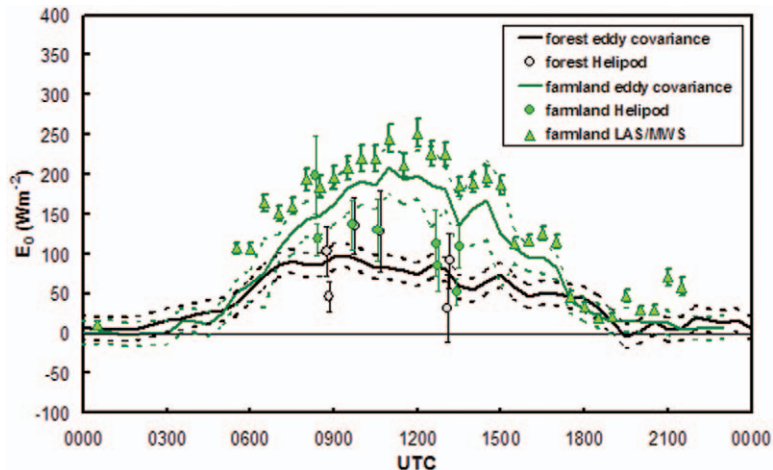


FIG. 7. Diurnal cycle of the latent heat fluxes above farmland and forest for 25 May 2003, measured by surface-based eddy covariance instrumentation, optical LAS and MWS, and the Helipod; uncertainty ranges for each of the measured fluxes are indicated by the dashed lines and error bars, respectively.

specifying appropriate parameters from lookup tables. Usually some tuning is inevitable to find reasonable coincidence between simulated and observed fluxes. The Multi-Objective Shuffled Complex Evolution Metropolis (MOSCEM) approach (Gupta et al. 1999; Vrugt et al. 2003) was used to calibrate three land surface schemes, namely, TERRA (Schrodin and Heise 2001), which is implemented in the weather forecast model [Lokal-Modell (LM)] of the DWD, the land surface scheme Surface Energy and Water Balance (SEWAB; Mengelkamp et al. 1999), and the land surface component of the Regional Model (REMO; Jacob 2001). Although identical parameters were chosen for all three SVATs, a large variation was found among the calibrated parameter sets that best fit the observations. In addition to characterizing soil and vegetation properties, the calibrated parameters also compensate for observational errors and model deficiencies. This results in different “best sets” of parameter values for the three different models.

So-called Pareto curves indicate the accordance of simulated and measured fluxes. Figure 8 shows the Pareto curves for the multiobjective calibration of the land surface scheme SEWAB for selected sites with latent and sensible heat fluxes as the objective functions. Among the various stations, the precision of the calibration (given by the length of the Pareto curve) and the accuracy of the simulation (given by the position) show some variation, but, with an rms below 50 W m^{-2} for the optimal parameter set (the point closest to the axis origin), the difference between

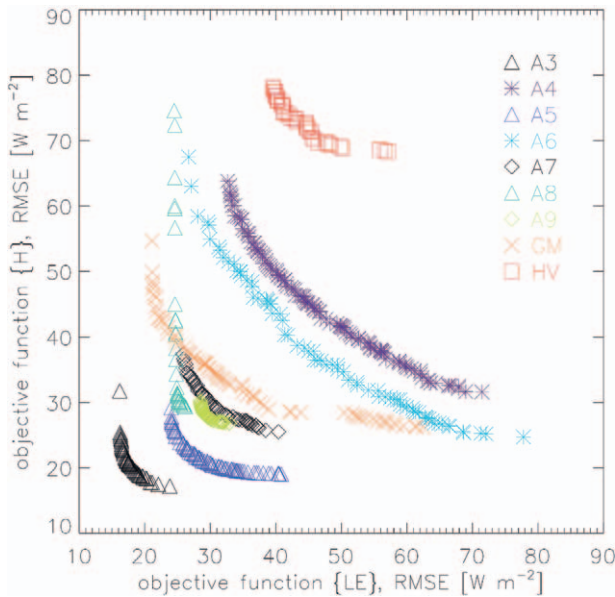


FIG. 8. Pareto curves for the SEWAB calibration for selected sites (A3: barley, A4: maize, A5: rye, A6: maize, A7: rape, A8: triticale, A9: rape, GM: grass, HV: pine forest).

simulated and observed fluxes is well within the uncertainty due to the energy balance closure gap.

REGIONAL-SCALE MODELS. The atmospheric boundary layer (ABL) structure was simulated using a suite of models ranging in resolution from the mesoscale to the large-eddy size. In particular, the regional climate model REMO (Jacob 2001; 18-km grid), the LM of the DWD (Steppeler et al. 2003; 7- and 1-km grid), the Flow Over Orographically Structured Terrain 3-Dimensional Köln (FOOT3DK) model of the University of Cologne (Heinemann and Kerschgens 2005) (1-km and 250-m grid), and a LES model of the University Hannover (Raasch and Harbusch 2001) were used. REMO is a three-dimensional hydrostatic atmospheric regional model, which is based on the former operational weather prediction model (Europamodell) of the DWD. The horizontal resolution is 18 km. The LM of the DWD is a fully compressible nonhydrostatic numerical weather prediction model, which is currently used with a horizontal resolution of 7 km for operational weather forecasts. For the current study, LM integrations with 7-km resolution (LM7) covering the whole LITFASS 2003 period, as well as high-resolution runs with 1-km horizontal resolution (LM1) for selected case studies, are used. The nonhydrostatic FOOT3DK model (version 3.10), developed at the University of Cologne, is run with horizontal resolutions of 1 km (F1) and 250 m (F250). A one-way-nesting procedure

is used for nesting the 250-m runs (F250) into the 1-km runs (F1).

STRUCTURE OF THE ATMOSPHERIC BOUNDARY LAYER.

Land surface heterogeneity affects the structure of the ABL at different scales. It can induce subgrid microscale and mesoscale circulations, which may influence cloud formation and the air–surface exchange (Giorgi and Avissar 1997; Heinemann and Kerschgens 2005). While very strong contrasts of, for example, temperature and energy fluxes can exist at very small scales at the surface itself, the overlying atmosphere produces an effective mixing and the surface contrasts eventually vanish at some height. The blending height concept of Mason (1988) is one common approach to describe this effect for small-scale surface heterogeneities. As outlined in the review paper of Mahrt (2000), the blending height concept may fail for convective conditions, when the blending height extends up to the ABL height. These conditions are often met for typical land use characteristics of the midlatitudes with heterogeneities of a few hundred meters. Thus, the development of surface-induced heterogeneities of the ABL structure on the scale of a few kilometers may be expected for midlatitude land use, as is typical for the LITFASS area. Heterogeneities in the LITFASS area are generally associated with land use, but a rain event occurring on 5 June 2003 was associated with a very heterogeneous precipitation pattern. Rain gauges in the LITFASS area measured 3–4 mm in the northeastern part, whereas up to 46 mm were measured in the southern part. This allows for investigating the differences between the heterogeneities resulting from land use patterns and heterogeneities induced by soil moisture patterns.

The contrast over the two land use types of farmland and forest is visible in the total heat flux profiles. The total flux is computed as the sum of dynamical (model resolved) and turbulent (parameterized) fluxes. For high-resolution simulations, only the profiles of the total flux coincide with typical flux profiles in the ABL (Heinemann 2006). The profiles of the total latent heat flux are shown in Fig. 9 at 1200 UTC for 25 and 30 May, and for 7 June for the F250 simulations. The farmland profiles are taken as the area average for a rectangle of 2.5 km × 14 km between the MOL and GM stations (Fig. 3), and the forest profiles represent the area average for a rectangle of 2.5 km × 12 km over the forest area in the western part. Prior to the rain event on 5 June, the contrast between farmland and forest is well defined on convective days. This is also shown for 25 May, when near-surface latent heat fluxes over

both surfaces are larger due to the higher soil moisture compared to that of 30 May. The latent heat flux profiles reflect the entrainment of dry air from the free atmosphere. An increase in the total latent heat flux is commonly seen in the lower ABL. It is mainly caused by the resolved fluxes, and is also found by the Helipod measurements. On 7 June, 2 days after the rain event, the farmland–forest contrast is not present in the F250 simulations (Fig. 9). Instead, we have a soil moisture–induced heterogeneity, with a pronounced contrast between the northeastern and the southeastern part of the LITFASS area. The two “north” and “south” boxes (both with a size of about 5 km × 5 km over the farmland area) illustrate this contrast.

SURFACE FLUXES FROM REGIONAL-SCALE MODELS.

Figure 10 shows the diurnal cycle (0500–1700 UTC) of the net radiation (Q_0) and latent heat flux (E_0) simulated by the different mesoscale models for the whole LITFASS area for 30 May 2003. Net radiation is almost identical for all three models, with a slight tendency to lower values for the LM. Despite this, the turbulent heat fluxes show large differences among the different models. The latent heat flux in REMO peaks at about 350 W m⁻², while the measurements show values of 100 W m⁻² during daytime. The operational LM version (LM op) tends to overestimate the latent heat flux.

When using the area-averaged means of LAI and plant cover derived from NOAA AVHRR data (Tittebrand et al. 2005) in the LM (version LM

NOAA) instead of the standard parameters, a significant improvement for the simulated latent heat flux is obtained. However, the latent heat flux is still significantly overestimated. The best coincidence with the measurements is achieved by the FOOT3DK model with a 250-m resolution and by “LM mosaic.” While F250 resolves most of the surface heterogeneities, LM mosaic uses the mosaic approach with a resolution of 7 km in the atmosphere and 1 km at the surface. A good candidate for explaining differences in the latent heat flux is the soil moisture in the models. Soil moisture is initialized differently in REMO and LM, and may therefore be one reason for the differences between those two. However, the improvement of the parameterization of land use and vegetation characteristics proves to be also very important. The wrong partitioning of the available energy into sensible and latent heat flux in REMO and LM op has important consequences for the ABL structure. It leads to a too shallow and too moist boundary layer as compared to lidar measurements.

With respect to the whole LITFASS period, LM op generally tends to overestimate the latent heat flux

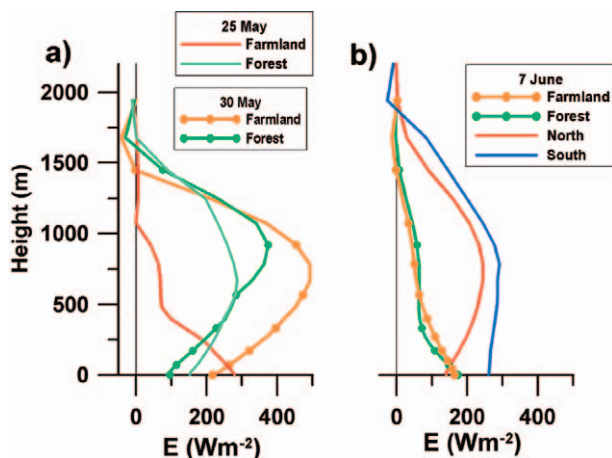


FIG. 9. Vertical profiles of the total latent heat flux of the FOOT3DK model with 250-m resolution (area averages of the sum of model-resolved and parameterized flux) at 1200 UTC for the farmland and forest boxes for three selected days [(left) 25 and 30 May, (right) 7 June]. (a) (b) The 7 June profiles for the north and south boxes are shown, in addition.

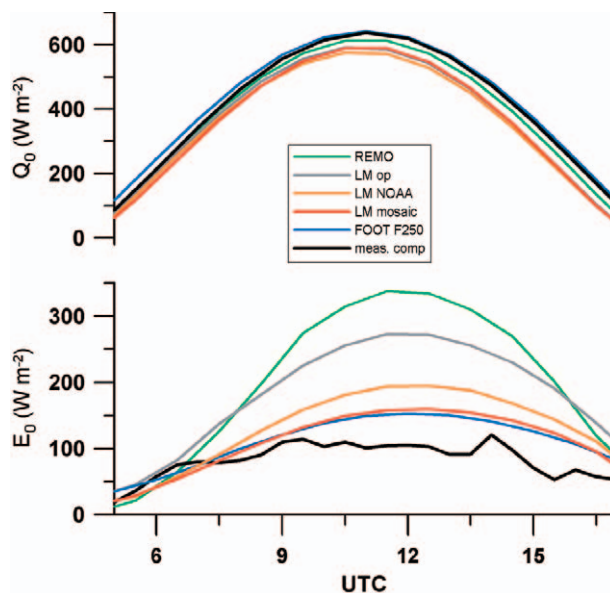


FIG. 10. Diurnal cycle of (top) Q_0 and (bottom) E_0 computed by different mesoscale models for the whole LITFASS area for 30 May 2003: REMO (18-km resolution), FOOT3DK (250-m resolution), different LM versions (7-km resolution), and area-averaged flux composite from the surface stations. The curves for the LM denote three different model runs: LM op is the operational run, LM NOAA uses LAI and vegetation cover derived from AVHRR, LM mosaic uses the mosaic method with 1-km resolution of the surface parameters.

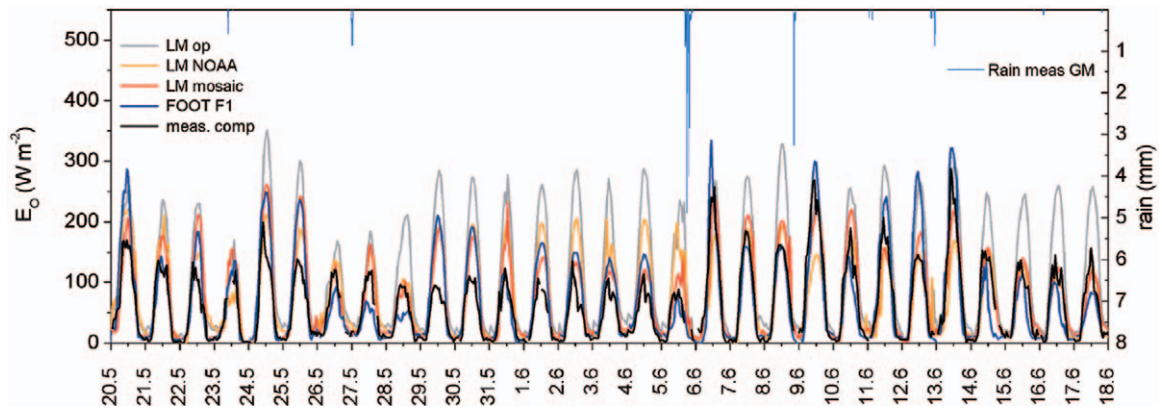


FIG. 11. Latent heat flux during LITFASS 2003 as simulated with different LM versions and FOOT3DK (1-km resolution) compared to the composite of measurements (hourly means). Precipitation is also indicated.

while the modified version with satellite-derived vegetation parameters (LM NOAA) shows a significant improvement (Fig. 11). With the mosaic approach implemented in the LM land surface scheme based on 1-km resolution subgrid-scale information for the albedo, stomatal resistance, and soil moisture, the agreement with the observed composite is much better. The quality of the LM mosaic run is comparable to the simulations of the FOOT3DK model with a resolution of 1 km.

SYNTHESIS. The EVA-GRIPS project focused on verifying the surface layer parameterization in atmospheric mesoscale models for heterogeneous land surfaces. A major field experiment during the growing season in May and June 2003, embedded into the operational measurement program of the Meteorological Observatory Lindenberg of the DWD, provided a comprehensive and unique dataset on land surface interaction processes over a heterogeneous land surface at the meso- γ scale. A complete quality-controlled time series of area-averaged fluxes for a 4-week period was created to be compared to the grid-scale flux simulations in numerical models.

Considerable variability was found among local surface fluxes (here we particularly focused on evaporation) over the major land use types across the area of the LITFASS 2003 experiment in dependence on both land use and meteorological forcing. But, large variations were also found between different types of agricultural farmland even on the same acre due to variations in soil wetness. Area-averaged surface fluxes calculated from the local measurements applying the tile approach were in good agreement with the area-representative values directly obtained from the scintillometer and Helipod measurements. When

comparing these fluxes with model simulations, the mosaic approach turned out to be a quite suitable way of estimating the grid cell-representative evaporation from subgrid information of the land use. Because all components of the surface energy and water balance were measured independently, the whole process chain could be consecutively compared to the corresponding simulated values. Adaptations in the soil moisture treatment in the regional model REMO and the operational weather forecast model LM resulted in an improved description of the energy partitioning in the land surface schemes of these models.

Large-eddy simulation studies also showed that mesoscale circulations contribute significantly to the area-averaged evaporation. This means that the local flux profile measurements as performed with remote sensing systems during LITFASS 2003 might not necessarily be representative for the mean ABL flux profiles. It seems advisable to perform a model study on mesoscale circulations during the design phase of the measurement strategy for future field experiments.

ACKNOWLEDGMENTS. The authors would like to express their gratitude to the German Ministry of Education and Research, which funded the project as part of the German Climate Research Program (DEKLIM) under Grant 01LD0103. Special thanks go to all those who assisted in the field experiment and to two anonymous reviewers for helpful comments.

REFERENCES

André, J. C., and Coauthors, 1988: Evaporation over land surfaces: First results from HAPEX-MOBILHY special observation period. *Ann. Geophys.*, **6**, 477–492.

- Araïn, A. M., J. D. Michaud, W. J. Shuttleworth, and A. J. Dolman, 1996: Testing of vegetation parameter aggregation rules applicable to the Biosphere-Atmosphere Transfer Scheme (BATS) at the Fife site. *J. Hydrol.*, **177**, 1–22.
- Avissar, R., 1992: Conceptual aspects of a statistical-dynamical approach to represent landscape sub-grid-scale heterogeneities in atmospheric models. *J. Geophys. Res.*, **97**, 2729–2742.
- , and R. A. Pielke, 1989: A parameterization of heterogeneous land surface for atmospheric numerical models and its impact on regional meteorology. *Mon. Wea. Rev.*, **117**, 2113–2136.
- Bange, J., and R. Roth, 1999: Helicopter-borne flux measurements in the nocturnal boundary layer over land—A case study. *Bound.-Layer Meteor.*, **92**, 295–325.
- , F. Beyrich, and D. A. M. Engelbart, 2002: Airborne measurements of turbulent fluxes during LITFASS-98: A case study about method and significance. *Theor. Appl. Climatol.*, **73**, 35–51.
- Beyrich, F., H.-J. Herzog, and J. Neisser, 2002a: The LITFASS project of DWD and the LITFASS-98 experiment: The project strategy and the experimental setup. *Theor. Appl. Climatol.*, **73**, 3–18.
- , H. A. R. de Bruin, W. M. L. Meijninger, J. W. Schipper, and H. Lohse, 2002b: Results from one-year continuous operation of a large aperture scintillometer over a heterogeneous landscape. *Bound.-Layer Meteor.*, **105**, 85–97.
- , and Coauthors, 2006: Area-averaged surface fluxes over the LITFASS region from eddy-covariance measurements. *Bound.-Layer Meteor.*, in press.
- Bolle, H. J., and Coauthors, 1993: EFEDA: European Field Experiment in a desertification threatened area. *Ann. Geophys.*, **11**, 173–189.
- Bösenberg, J., 1998: Ground-based differential absorption lidar for water-vapor and temperature profiling: Methodology. *Appl. Opt.*, **37**, 3845–3860.
- Chehbouni, A., E. G. Njoku, J.-P. Lhomme, and Y. H. Kerr, 1995: Approaches for averaging surface parameters and fluxes over heterogeneous terrain. *J. Climate*, **8**, 1386–1393.
- Foken, T., and S. P. Oncley, 1995: Workshop on instrumental and methodological problems of land-surface flux measurements. *Bull. Amer. Meteor. Soc.*, **76**, 1191–1193.
- Foken, Z., M. Göckede, M. Mauder, L. Mahrt, B. D. Amiro, and J. W. Munger, 2004: Post-field data quality control. *Handbook of Micrometeorology: A Guide for Surface Flux Measurements*, X. Lee, W. Massman, and B. E. Law, Eds., Kluwer, 181–208.
- Giorgi, F., and R. Avissar, 1997: Representation of heterogeneity effects in earth system modeling: Experience from land surface modeling. *Rev. Geophys.*, **35**, 413–438.
- Goutorbe, J.-P., and Coauthors, 1994: HAPEX-Sahel: A large-scale study of land-atmosphere interactions in the semi-arid tropics. *Ann. Geophys.*, **12**, 53–64.
- Gupta, H. V., L. A. Bastidas, S. Sorooshian, W. J. Shuttleworth, and Z. L. Yang, 1999: Parameter estimation of a land surface scheme using multicriteria methods. *J. Geophys. Res.*, **104** (D16), 19 491–19 503.
- Halldin, S., L. Gottschalk, A. A. van de Griend, S. E. Gryning, M. Heikinheimo, U. Högström, A. Jochum, and L. C. Lundin, 1998: NOPEX—A northern hemisphere climate processes land surface experiment. *J. Hydrol.*, **212–213**, 172–187.
- , S.-E. Gryning, and C. R. Lloyd, 2001: Land-surface/atmosphere exchange in high-latitude landscapes. *Theor. Appl. Climatol.*, **70** (Special Issue), 1–3.
- Heinemann, G., 2006: On the consideration of meso-scale transports in climate modelling. *Theor. Appl. Climatol.*, **83**, 35–50.
- , and M. Kerschgens, 2005: Comparison of methods for area-averaging surface energy fluxes over heterogeneous land surfaces using high-resolution non-hydrostatic simulations. *Int. J. Climatol.*, **25**, 379–403.
- Jacob, D., 2001: A note on the simulation of the annual and interannual variability of the water budget over the Baltic Sea drainage basin. *Meteor. Atmos. Phys.*, **77**, 61–73.
- Johnsen, K.-P., H.-T. Mengelkamp, and S. Huneke, 2005: Multi-objective calibration of the land surface scheme TERRA/LM using LITFASS-2003 data. *Hydrol. Earth. Syst. Sci.*, **9**, 576–585.
- Koster, R. D., and M. J. Suarez, 1992a: A comparative analysis of two land surface heterogeneity representations. *J. Climate*, **5**, 1379–1390.
- , and —, 1992b: Modeling the land surface boundary in climate models as a composite of independent vegetation stands. *J. Geophys. Res.*, **97** (D3), 2697–2715.
- LeMone, M. A., and Coauthors, 2000: Land-atmosphere interaction research, early, results and opportunities in the Walnut River watershed in southeast Kansas: CASES and ABLE. *Bull. Amer. Meteor. Soc.*, **81**, 757–779.
- Lhomme, J.-P., A. Chehbouni, and B. Monteny, 1994: Effective parameters of surface energy balance in heterogeneous landscape. *Bound.-Layer Meteor.*, **71**, 297–309.
- Li, B., and R. Avissar, 1994: The impact of spatial variability of land-surface characteristics on land-surface heat fluxes. *J. Climate*, **7**, 527–537.
- Linné, H., B. Hennemuth, J. Bösenberg, and K. Ertel, 2005: Water vapour flux profiles in the convective boundary layer. *Theor. Appl. Climatol.*, in press.

- Mahrt, L., 2000: Surface heterogeneity and vertical structure of the boundary layer. *Bound.-Layer Meteor.*, **96**, 33–62.
- Mason, P. J., 1988: The formation of areally-averaged roughness length. *Quart. J. Roy. Meteor. Soc.*, **114**, 399–420.
- Mengelkamp, H.-T., 2004: Land surface modelling in BALTEX. *GEWEX News*, Vol. 14, No. 3, August 2004, 7.
- , K. Warrach, and E. Raschke, 1999: SEWAB—A parameterization of the Surface Energy and Water Balance for atmospheric and hydrologic models. *Adv. Water Res.*, **23**, 165–175.
- Noilhan, J., P. Lacarrere, A. J. Dolman, and E. M. Blyth, 1997: Defining area-average parameters in meteorological models for land surfaces with mesoscale heterogeneity. *J. Hydrol.*, **190**, 302–316.
- Pielke, R. A., and R. Avissar, 1990: Influence of landscape structure on local and regional climate. *Landscape Ecol.*, **4**, 133–155.
- Raasch, S., and G. Harbusch, 2001: An analysis of secondary circulations and their effects caused by small-scale surface inhomogeneities using large-eddy simulation. *Bound.-Layer Meteor.*, **101**, 31–59.
- Raschke, E., and Coauthors, 2001: The Baltic Sea Experiment (BALTEX): A European contribution to the investigation of the energy and water cycle over a large drainage basin. *Bull. Amer. Meteor. Soc.*, **82**, 2389–2413.
- Schrodin, R., and E. Heise, 2001: The multi-layer-version of the DWD soil model TERRA/LM. Consortium for Small-Scale Modelling (COSMO) Tech. Rep. 2, 16 pp.
- Sellers, P. J., and F. G. Hall, 1992: FIFE in 1992: Results, scientific gains, and future research directions. *J. Geophys. Res.*, **97**, 19 091–19 109.
- , M. D. Heiser, F. G. Hall, S. B. Verma, R. L. Desjardins, P. M. Schuepp, and J. I. MacPherson, 1997a: The impact of using area-averaged land surface properties—topography, vegetation condition, soil wetness—in calculations of intermediate scale (approximately 10 km²) surface-atmosphere heat and moisture fluxes. *J. Hydrol.*, **190**, 269–301.
- , and Coauthors, 1997b: BOREAS in 1997: Experiment overview, scientific results, and future directions. *J. Geophys. Res.*, **102**, 28 731–28 769.
- Shuttleworth, W. J., Z.-L. Yang, and M. A. Arain, 1997: Aggregation rules for surface parameters in global models. *Hydrol. Earth Syst. Sci.*, **2**, 217–226.
- Steppele, J., G. Doms, U. Schuettler, H. W. Bitter, A. Gassmann, E. Damrat, and G. Gregoric, 2003: Mesogamma scale forecasts using the nonhydrostatic model LM. *Meteor. Atmos. Phys.*, **82**, 75–96.
- Tittebrand, A., A. Schwiebus, and F. H. Berger, 2005: The influence of land-surface parameters on energy flux densities derived from remote sensing data. *Meteor. Z.*, **14**, 227–236.
- Vrugt, J. A., H. V. Gupta, L. A. Bastidas, W. Bouten, and S. Sorooshian, 2003: Effective and efficient algorithm for multiobjective optimisation of hydrologic models. *Water Res. Res.*, **39**, 1214, doi:10.1029/2002WR001746.
- Wetzel, P. J., and J.-T. Chang, 1988: Evapotranspiration from nonuniform surfaces: A first approach for short-term numerical prediction. *Mon. Wea. Rev.*, **116**, 600–621.
- Wilczak, J. M., S. P. Oncley, and S. A. Stage, 2001: Sonic anemometer tilt correction algorithms. *Bound.-Layer Meteor.*, **99**, 127–150.
- Wilson, K., and Coauthors, 2002: Energy balance closure at FLUXNET sites. *Agric. For. Meteorol.*, **113**, 223–243.